A Wavelet-Based Method for Detection and Classification of Single and Crosscountry Faults in Transmission Lines

F. B. Costa, B. A. Souza, and N. S. D. Brito

Abstract— **This paper presents a discrete wavelet transform approach to detect and classify faults in transmission lines by the analysis of oscillographic records. Most of the existing methods treat the fault as a single type. Thus, the performance of these methods might be limited for real applications in power systems. In this framework, the proposed approach overcomes this problem by the ability to detect and classify faults in actual oscillographic data with either single or crosscountry fault. Sliding data windows on the wavelet coefficients with length equivalent to one cycle of the fundamental power frequency are used to achieve wavelet coefficient energies for detection and classification tasks. The performance of the method was evaluated for both actual and simulated data and good results were achieved.**

Index Terms— **Fault, transmission lines, wavelet transform.**

I. INTRODUCTION

A Fault on a power system is an abnormal condition that involves an electrical failure of power system equipament operating at one of the primary voltages. Postanalysis of the fault has become an important issue, because it can provide helpful information for system operators to make decisions about the system restoration and to get specific information regarding the operation of the protection system.

The *oscillography* is vital to the operation of an electrical power system, because it provides the automatic monitoring in transmission lines and supplies information of faults and power quality (PQ) disturbances into *oscillographic data* recorded by equipments such as digital fault records (DFR). The interconnection among these equipments forms the *oscillographic network* (Fig. 1) [1].

The DFR must register faults, PQ disturbances, and normal maintenance operations, such as: line energization and deenergization. However, these equipments sometimes also register a lot of data that may not correspond to a transient event. In this way, the amount of data can be extremely large and the manual visual inspection by system operators becomes impossible. Therefore, an automatic method installed in a *master station* is necessary to detect and classify fault and transient disturbances by the oscillographic record analysis, keeping only relevant information for the oscillography's main purpose.

This work was supported by Brazilian National Research Council (CNPq) and CHESF.

The authors are with Department of Electrical Engineering at Federal University of Campina Grande, 882 Aprígio Veloso Av, Bodocongó, Campina Grande - PB, CEP:58.109-970, Brazil. E-mail: {flabc, benemar, nubia}@ee.ufcg.edu.br.

Presented at the International Conference on Power Systems Transients (IPST'09) in Kyoto, Japan on June 3-6, 2009.

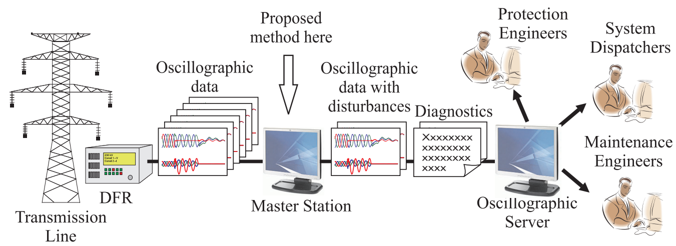

Fig. 1. Oscillographic network schedule to gather records.

Discrete wavelet transform (DWT) has been recommended for analysis of signals that have fast changes, such as transient phenomena associated with power system disturbances [2]. In this way, many researches have focused on wavelet-based techniques applied to analyze switching transients [3], to detect and classify PQ disturbances [4], [5] and faults [6], [7].

Most of the existing methods treat the faults as a single type, limiting their performance in real applications. Sometimes, a single line-to-ground (SLG) fault can engulf a second phase where it changes to a double line-to-ground (DLG) fault. A fault that change in type during a fault period is called *crosscountry* fault. This paper proposes a method for single and crosscountry fault detection and classification.

The method is based on the detail coefficient energies of the currents achieved by sliding data windows with length equivalent to one cycle of the fundamental power frequency and only the first wavelet scale is used. The performance of the method has been evaluated for both actual and simulated data and good results have been achieved. All actual oscillographic records were measured by power line monitoring devices from Hydro Electric Company of San Francisco (CHESF), a Brazilian utility company, and a software-based method is installed in some master stations.

II. DISCRETE WAVELET TRANSFORM

The DWT is a powerful time-frequency method to analyze a signal within different frequency ranges, by means of dilating and translating of a single function named *mother wavelet* [8].

According to Mallat's algorithm, the DWT uses the high-pass $h(k)$ and the low-pass $g(k)$ filters to divide the frequency-band of the input signal into high- and low-frequency components [9]. This operation may be repeated recursively, feeding the down-sampled low-pass filter output into another identical filter pair, decomposing the signal into approximation $c(k)$ and wavelet $d(k)$ coefficients for various scales of resolution, as follows:

$$c_j(k) = \sum_n h(n-2k)c_{j-1}(n), \quad (1)$$

$$d_j(k) = \sum_n g(n-2k)c_{j-1}(n), \quad (2)$$

where j is the wavelet scale.

In each scale, $h(k)$ and $g(k)$ filter the input signal of this scale, yielding new approximation and detail coefficients, respectively. Thus, this process divides the frequency spectrum of the original signal into octave bands [8]. In addition, the Nyquist theorem states that a discrete signal with sampling rate of f_s has frequency components limited from 0 until $f_s/2$. Therefore, the frequency spectrum of the wevelet coefficient at scale j is:

$$[f_s/2^{2j}, f_s/2^j]. \quad (3)$$

The coefficients of the filter pair are associated with the selected mother wavelet. The mother wavelet Daubechies 4 (db4) [8] has been found suitable to be embedded with the proposed algorithm, due to its good time resolution that provides an accurate detection of the fast transients [7], [10].

A. Energy of the Detail Coefficients

Consider d_j the wavelet coefficients, at scale j, of an input signal with sampling rate of f_s. In order to compute the wavelet coefficient energies, a sliding data window goes through d_j, shifting one coefficient at a time, viz [5], [11]

$$\mathcal{E}(k) = \begin{cases} \sum_{n=1}^{\Delta k/2^j} d_j^2(n), & \text{if} \quad 1 \leqslant k \leqslant \frac{\Delta k}{2^j} \\ \sum_{n=k-\Delta k/2^j+1}^{k} d_j^2(n), & \text{if } \frac{\Delta k}{2^j} < k \leqslant \frac{k_T}{2^j} \end{cases} \quad (4)$$

where: Δk is the window length, $k = \{1, 2, \ldots, k_T/2^j\}$, and k_T is the total number of samples of the input signal. In this paper, Δk is the amount of samples contained in one cycle of the fundamental power frequency, as follows:

$$\Delta k = f_s/f. \quad (5)$$

III. PROPOSED METHOD

The proposed disturbance diagnostic approach involves two modules (Fig. 2) described as follow:

- The first module is related to disturbance detection, proposed by [11]. The method gets the voltage and current samples from the oscillographic record. The DWT is applied and the wavelet coefficient energy waveform for each signal is computed by (4), with j=1 (first scale). The transient disturbance detection is carried out through the analysis of the wavelet coefficient energy curves of the phase currents. Besides faults, the method detects other kinds of transient disturbances like voltage sags and switching transients. In addition, for instance, a fault followed by a line reclosing in just one oscillographic data (multiple disturbances) are also detected and identified.
- The second module, proposed in this paper, achieves the fault classification when a fault is detected in the first module. In addition, the proposed method also classifies crosscountry faults.

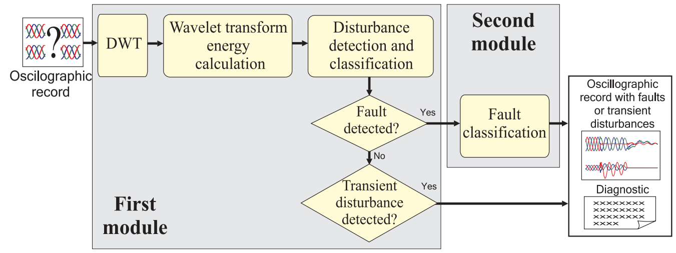

Fig. 2. Flowchart of the proposed method.

IV. FAULT CLASSIFICATION METHOD

The features of the voltage and current waveforms before, during, and after a transmission line fault may be significantly different. Fig. 3 depicts the phase voltages and currents related to an actual crosscountry fault, whose type changed from a BG to a BCG fault. The following instants are characterized by transient inception:

1) k_o: sample related to the fault inception.
2) k_1: sample in which the fault changes its type.
3) k_2: sample related to the fault clearance.

According to Fig. 3, the BG fault starts at sample k_o (fault inception point) and changes its type to a BCG fault at sample k_1. Fig. 4 depicts the wavelet coefficient energy waveforms of the phase currents, at first scale.

Besides the fault detection, the fault inception and clearance samples are also estimated by [11] through the analysis of the wavelet coefficient energies. Fault detection and location are based on rising energy variation (Fig. 4). In the same way, the fault exchange is located through a rising energy variation between fault inception and clearance (Fig. 4).

A. Fault Coordinates

Based on statistical analysis, [11] states that the wavelet coefficient energies of the phase and neutral currents ($\mathcal{E}_A(k)$, $\mathcal{E}_B(k)$, $\mathcal{E}_C(k)$ and $\mathcal{E}_G(k)$) before fault inception ($k_o/2$) are almost constant and can be approximated by the following equations:

$$\mathcal{E}_A(k) = E_{pre\_IA}, \quad (6)$$

$$\mathcal{E}_B(k) = E_{pre\_IB}, \quad (7)$$

$$\mathcal{E}_C(k) = E_{pre\_IC}, \quad (8)$$

$$\mathcal{E}_G(k) = E_{pre\_IG}, \quad (9)$$

where $k < k_o/2$.

E_{pre_IA}, E_{pre_IB}, E_{pre_IC} and E_{pre_IG} are due to electrical noises and have a small value between E_1=1e^{-6} and E_2=8e^{-5}.

Soon after fault inception, the energy values rise due to the transient effects. The increasing of energy at point k is given by:

$$d\mathcal{E}_A(k) = (\mathcal{E}_A(k) - E_{pre\_IA})/E_{pre\_IA}, \quad (10)$$

$$d\mathcal{E}_B(k) = (\mathcal{E}_B(k) - E_{pre\_IB})/E_{pre\_IB}, \quad (11)$$

$$d\mathcal{E}_C(k) = (\mathcal{E}_C(k) - E_{pre\_IC})/E_{pre\_IC}, \quad (12)$$

$$d\mathcal{E}_G(k) = (\mathcal{E}_G(k) - E_{pre\_IG})/E_{pre\_IG}, \quad (13)$$

where $k \geqslant k_o/2$.

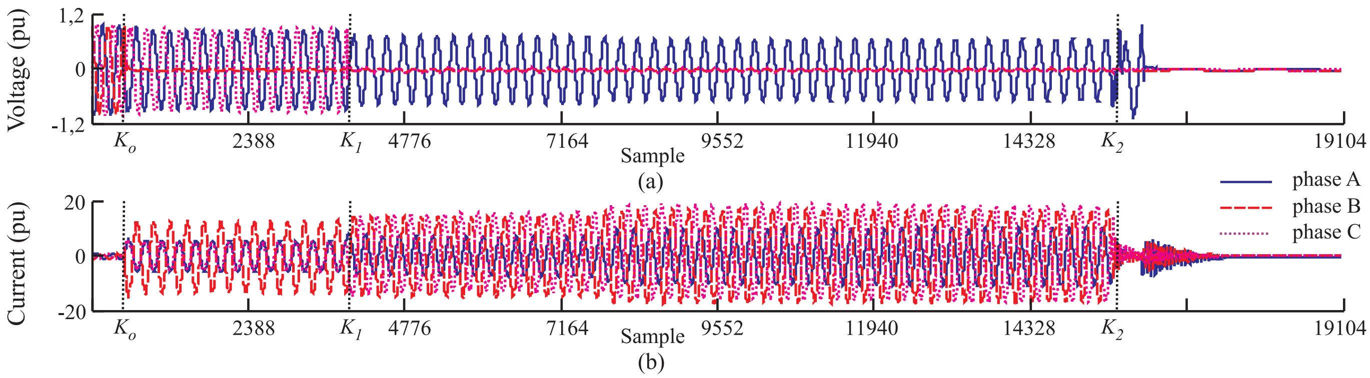

Fig. 3. Actual oscillographic record related to a crosscountry fault: (a) normalized phase voltages; (b) normalized phase currents.

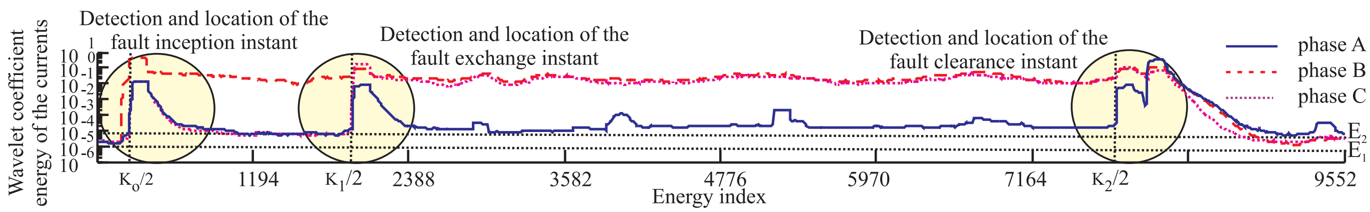

Fig. 4. Wavelet coefficient energies of the phase voltages and currents, at scale 1.

$A(k)$, $B(k)$, $C(k)$ and $G(k)$ are the normalized variables from $d\mathcal{E}_A(k)$, $d\mathcal{E}_B(k)$, $d\mathcal{E}_C(k)$ and $d\mathcal{E}_G(k)$, respectively, as follows:

$$A(k) = d\mathcal{E}_A(k)/(d\mathcal{E}_A(k) + d\mathcal{E}_B(k) + d\mathcal{E}_C(k)), \tag{14}$$

$$B(k) = d\mathcal{E}_B(k)/(d\mathcal{E}_A(k) + d\mathcal{E}_B(k) + d\mathcal{E}_C(k)), \tag{15}$$

$$C(k) = d\mathcal{E}_C(k)/(d\mathcal{E}_A(k) + d\mathcal{E}_B(k) + d\mathcal{E}_C(k)), \tag{16}$$

$$G(k) = d\mathcal{E}_G(k)/(d\mathcal{E}_A(k) + d\mathcal{E}_B(k) + d\mathcal{E}_C(k)). \tag{17}$$

According to Eqs. (14), (15), (16) and (17):

$$A(k) + B(k) + C(k) = 1, \tag{18}$$

where $0 \leqslant A(k) \leqslant 1$, $0 \leqslant B(k) \leqslant 1$, $0 \leqslant C(k) \leqslant 1$, $G(k) \geqslant 0$ and $k \geqslant k_o/2$.

The proposed classification method is based on a three dimensional coordinate system which is composed by three perpendicular axes to each other. The coordinates of this system (*fault coordinates*) are in the form ($A(k)$, $B(k)$, $C(k)$), computed by Eqs. (14), (15) and (16). According to Eq. (18), the coordinates are located on a three dimensional plane, called *fault plane*.

B. Unsymmetrical Fault Planes

The fault coordinates for each fault type are located on distinctive regions on fault planes. Fault planes related to the SLG, line-to-line (LL), and DLG faults will be dealt with in this section.

Ideally, the electromagnetic coupling effects among conductors can be neglected. Thus, after fault inception ($k \geqslant k_o/2$), the fault coordinates relate to AG ideal faults would be ($A(k)$=1, $B(k)$=0, $C(k)$=0) and $G(k)$=1, because there are no transients on B and C phase currents.

With regard to AG faults, assume that $A(k)>B(k)>C(k)$. Taking into account $B(k)$ tending to $C(k)$ ($A(k) - B(k) > B(k) - C(k)$) and $A(k)+B(k)+C(k)=1$, $B(k) < 1/3$ is obtained. Therefore, $A(k)>B(k)>C(k)$ with $B(k) < 1/3$ and $A(k) > C(k) > B(k)$ with $C(k) < 1/3$ delimit the AG fault plane under plane equation $A(k)+B(k)+C(k)=1$. In the same way, the BG and CG fault planes can be identified (Fig. 5).

With regard to AB faults, assume again that $A(k)>B(k)>C(k)$. Taking into account $B(k)$ tending to $A(k)$ ($A(k)-B(k) \leqslant B(k)-C(k)$) and $A(k)+B(k)+C(k)=1$, the value $B(k) \geqslant 1/3$ is now obtained. $B(k)>A(k)>C(k)$ with $A(k) \geqslant 1/3$ delimits the AB fault plane too. In the same way, the AC and BC fault planes can be identified (Fig. 5).

The LL fault planes and DLG fault planes are the same. The ground coordinate $G(k)$ is used to distinguish these kinds of faults. For SLG and DLG faults, $G(k) \approx 1$ was observed. On the other hand, $G(k) < 1$ was observed for LL faults.

Fig. 5 also depicts the fault coordinates in one cycle soon after $k_o/2$ and $k_1/2$, of the crosscountry fault energy waveforms of the Fig. 4. The fault coordinates after $k_o/2$ are located on BG fault plane and the fault coordinates after $k_1/2$ are located on BC fault plane. Therefore, these coordinates indicate a BG+BCG fault. The proposed classification method uses these fault coordinates to identify the fault type.

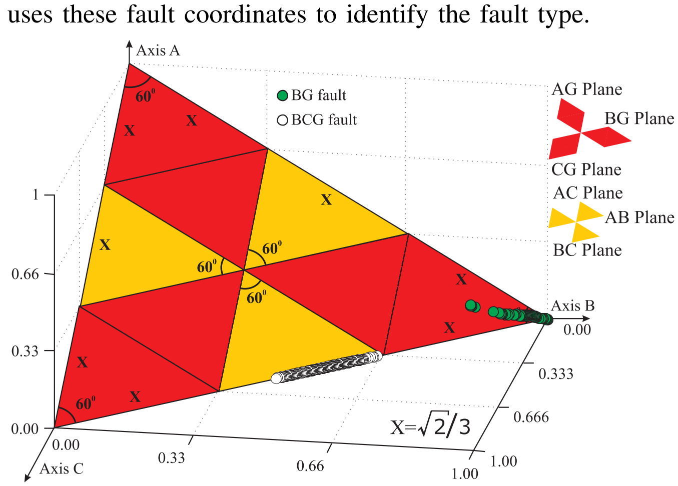

Fig. 5. one-phase and two-phase fault planes.

The regions of the fault planes (Fig. 5) were identified by using geometry and they are summarized in Tab. I.

TABLE I

FAULT TYPE ACCORDING TO ITS COORDINATES.

Coordinate values	Fault type	Coordinate values	Fault type
B<1/3, C<1/3	AG	$A \geqslant 1/3$, $B \geqslant 1/3$	AB or ABG
A<1/3, C<1/3	BG	$B \geqslant 1/3$, $C \geqslant 1/3$	BC or BCG
A<1/3, B<1/3	CG	$A \geqslant 1/3$, $C \geqslant 1/3$	AC or ACG

C. Symmetrical Fault Planes

Three-phase faults are known as symmetrical faults. Roughly 5 % of all short-circuits involve all three phases. The fault coordinates of this disturbance are in accordance with the fault inception angle and they can be located on any aforementioned fault plane. The ground component $G(k)$ is used to distinguish the symmetrical and unsymmetrical faults.

The simplified single-phase short line model depicted in Fig. 6 was used in order to identify the fault inception angle effects on the fault currents. The transmission line was modeled as resistances (R_1 and R_2) and inductances (L_1 and L_2), the load was modeled as a constant impedance (R_{Load} and L_{Load}) and, the fault was modeled as a switch followed by a constant resistance (R_{fault}).

For ease of description, the switch will be closed on sample k=k_o and the voltage phase angle in this time will be φ+θ_o. In this way, the local voltage ($v_A(k)$) was represented as follows:

$$v_A(k) = V cos\left(\frac{w(k-k_o)}{f_s} + \theta_o + \varphi\right). \tag{19}$$

Before fault inception, the current in normal operation is given by:

$$i_A(k) = \frac{V}{|Z|} cos\left(\frac{w(k-k_o)}{f_s} + \theta_o\right), \tag{20}$$

where:

$$|Z| = \sqrt{(R_1 + R_2 + R_{load})^2 + w^2(L_1 + L_2 + L_{load})^2}, \tag{21}$$

$$\varphi = tg^{-1}\frac{w(L_1 + L_2 + L_{load})}{R_1 + R_2 + R_{load}}. \tag{22}$$

According to Eq. (20), θ_o is the fault inception angle by taking into account i_A as reference.

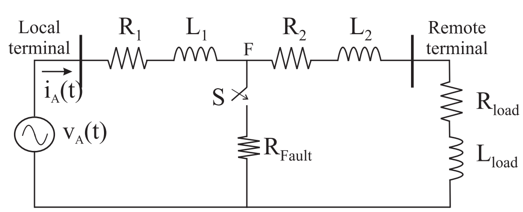

Fig. 6. Single-phase short distance fault line model.

For ease of description, the fault resistance is disregarded. Neglecting all harmonic components and fault-induced transients, the current at local end after fault inception ($k \geqslant k_o$) might be expressed as:

$$i_A(k) = \frac{V}{|Z_f|} cos\left(\frac{w(k-k_o)}{f_s} + \theta_o + \varphi - \varphi_f\right) + I_o e^{\frac{-(k-k_o)R_1}{f_s L_1}}, \tag{23}$$

where:

$$|Z_f| = \sqrt{R_1^2 + w^2 L_1^2}, \tag{24}$$

$$\varphi_f = tg^{-1}\frac{wL_1}{R_1}. \tag{25}$$

The first term of Eq. (23) is a sinusoidal function. It is related to a new steady-state operation after fault inception. The second term is nonperiodic and decays exponentially with a time constant R_1/L_1. This nonperiodic term is called *dc offset*.

The dc offset magnitude at fault inception (k=k_o) is I_o, which is computed as follows:

$$I_o = \frac{V}{|Z|} cos(\theta_o) - \frac{V_A}{|Z_f|} cos(\theta_o + \varphi - \varphi_f), \tag{26}$$

According to Eq. (26), the magnitude of the dc offset at fault inception (I_o) depends of various parameters: fault location (R_1 and L_1), system loading (R_{load} and L_{load}), and the fault inception angle (θ_o). Considering a fixed load impedance and fault location, I_o is in accordance with the fault inception angle in a sinusoidal way, as follows:

$$I_o = \mathcal{I} cos(\theta_o - \alpha), \tag{27}$$

where $\mathcal{I}$ and α are constants.

The wavelet coefficients at first scale have frequency spectrum of [$f_s/4$, $f_s/2$]. In this way, only the fault-induced transients could affect the wavelet coefficient values after fault inception (k>k_o). On the other hand, the dc offset is composed by low frequency components, but due to its shape it affects the wavelet coefficient value at fault inception (k=$k_o/2$). According to the aforementioned conditions, the fault-induced transients were neglected and the wavelet coefficient of I_A at fault inception can be expressed as:

$$d_A(k_o/2) = \mathcal{D}_A cos(\theta_o - \alpha). \tag{28}$$

where $\mathcal{D}_A$ and α are constants.

Due to electrical noise on the currents in steady-state operation, the energy values related to I_A can be approximated to E_{pre_IA} (Eq. (6)) before fault inception. Therefore, according to Eqs. (4) and (28) the energy of the wavelet coefficients of this current, at first scale, can be expressed as:

$$\mathcal{E}_A(k) \approx \begin{cases} E_{pre\_IA}, & \text{if } k < k_o/2 \\ \mathbb{E}_A cos^2(\theta_o - \alpha), & \text{if } k_o/2 \leqslant k \leqslant (k_o + \Delta k)/2 \end{cases} \tag{29}$$

where $\mathbb{E}_A$ is a constant.

Neglecting the electromagnetic coupling effects among conductors in a simplified three-phase line model, each phase line can be modeled as Fig. 6, according to the phase lag of 120^o. In this way, the energy of the wavelet coefficients of I_B and I_C, can be expressed as

$$\mathcal{E}_B(k) \approx \begin{cases} E_{pre\_IB}, & \text{if } k < k_o/2 \\ \mathbb{E}_B cos^2(\theta_o - \alpha), & \text{if } k_o/2 \leqslant k \leqslant (k_o + \Delta k)/2 \end{cases} \tag{30}$$

$$\mathcal{E}_C(k) \approx \begin{cases} E_{pre\_IC}, & \text{if } k < k_o/2 \\ \mathbb{E}_C cos^2(\theta_o - \alpha), & \text{if } k_o/2 \leqslant k \leqslant (k_o{+}\Delta k)/2 \end{cases} \tag{31}$$

According to Eqs. 10, 11, 12 and 14, the fault coordinate A at fault inception (k=$k_o/2$) can be expressed as

$$A(k) = \frac{(\mathcal{E}_A(k) - E_{pre\_IA})/E_{pre\_IA}}{\frac{\mathcal{E}_A(k) - E_{pre\_IA}}{E_{pre\_IA}} + \frac{\mathcal{E}_B(k) - E_{pre\_IB}}{E_{pre\_IB}} + \frac{\mathcal{E}_C(k) - E_{pre\_IC}}{E_{pre\_IC}}}, \tag{32}$$

Considering $\mathcal{E}_A(k_o/2) \gg E_{pre\_IA}$, $\mathcal{E}_B(k_o/2) \gg E_{pre\_IB}$ and $\mathcal{E}_C(k_o/2) \gg E_{pre\_IC}$ and $E_{pre\_IA} \approx E_{pre\_IB} \approx E_{pre\_IC}$. Therefore, Eq. (32) can be expressed as:

$$A(k_o/2) = \frac{\mathcal{E}_A(k_o/2)}{\mathcal{E}_A(k_o/2) + \mathcal{E}_B(k_o/2) + \mathcal{E}_C(k_o/2)}, \tag{33}$$

or

$$A = \frac{\mathbb{E}_A cos^2(\theta_o - \alpha)}{\mathbb{E}_A cos^2(\theta_o - \alpha) + \mathbb{E}_B cos^2(\theta_o - 60^o - \alpha) + \mathbb{E}_C cos^2(\theta_o + 60^o - \alpha)} \tag{34}$$

In the simplified three-phase line model without electromagnetic coupling, the phase currents are under the same situations with the respective phase lags. In this way, $\mathbb{E}_A \approx \mathbb{E}_B \approx \mathbb{E}_C$. In addition, $cos^2(\theta_o - \alpha) + cos^2(\theta_o - 60^o - \alpha) + cos^2(\theta_o + 60^o - \alpha) = 3/2$. The ideal fault coordinates in a three-phase fault, at fault inception, are given by:

$$A(k_o/2) = \frac{2}{3} cos^2(\theta_o - \alpha), \tag{35}$$

$$B(k_o/2) = \frac{2}{3} cos^2(\theta_o - 60^o - \alpha), \tag{36}$$

$$C(k_o/2) = \frac{2}{3} cos^2(\theta_o + 60^o - \alpha), \tag{37}$$

$$G(k_o/2) = 0. \tag{38}$$

After fault inception (k>$k_o/2$), the energy magnitudes are due to the fault-induced transients and the fault coordinates are also computed according to Eqs. (35), (36) and (37).

Fig. 7 depicts the fault plane related to the three-phase faults. The coordinates may be localized around a circle, according to the fault inception angle (Eqs. (35), (36) and (37)). However, the proposed method identify a three-phase fault located on any position when $G(k) < 0.2$. Otherwise, the fault corresponds a unsymmetrical fault.

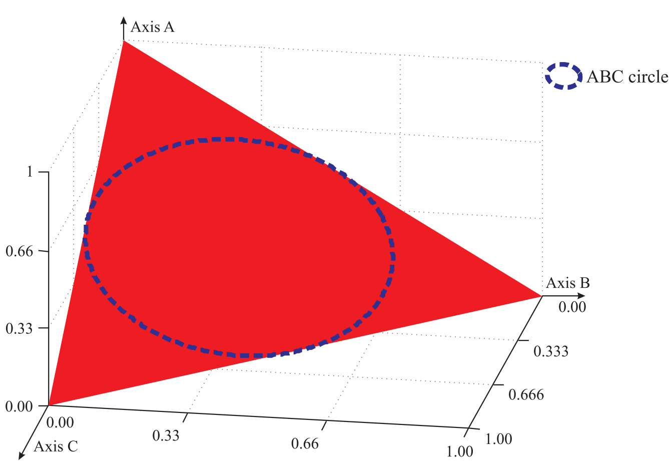

Fig. 7. one-phase and two-phase fault planes.

D. Fault Classification Rules

Tab. II summarizes the classification auxiliar parameters.

TABLE II
AUXILIARY PARAMETERS FOR FAULT CLASSIFICATION.

Parameters				Type	Parameters				Type
a	b	c	g	of fault	a	b	c	g	of fault
1	0	0	1	AG fault	1	1	0	1	ABG fault
0	1	0	1	BG fault	0	1	1	1	BCG fault
0	0	1	1	CG fault	1	0	1	1	ACG fault
1	1	0	0	AB fault	1	1	1	-	ABC fault
0	1	1	0	BC fault					
1	0	1	0	AC fault					

The fault classification method is summarized as follows:

1) Do $k = (k_o{+}\triangle k)/2$ (fault coordinates located one cycle after fault inception).
2) Set a=0, b=0, c=0 and g=0 (variables related to fault type).
3) Get the fault coordinates ($A(k)$, $B(k)$, $C(k)$) and $G(k)$.
4) If $G(k) < 0.2$, so $a = b = c = 1$.
5) Otherwise, if $B(k) < 1/3$ and $C(k) < 1/3$, so a=g=1.
6) Otherwise, if $A(k) < 1/3$ and $C(k) < 1/3$, so b=g=1.
7) Otherwise, if $A(k) < 1/3$ and $B(k) < 1/3$, so c=g=1.
8) Otherwise, if $A(k) \geqslant 1/3$ and $B(k) \geqslant 1/3$, so a=b=1.
9) Otherwise, if $B(k) \geqslant 1/3$ and $C(k) \geqslant 1/3$, so b=c=1.
10) Otherwise, if $A(k) \geqslant 1/3$ and $C(k) \geqslant 1/3$, so a=c=1.
11) If $a + b + c = 2$ and $0.2 \leqslant G(k) \leqslant 0.8$, so g=1 (DLG fault).
12) Classify the fault according to obtained values a, b, c and g, and the Tab. II.
13) If a+b+c=3 (three-phase fault), then finish the analysis.
14) Otherwise, if a fault changing was detected, get the fault coordinates in one cycle after the changing time and go to step 3.
15) Otherwise, finish the analysis.

V. PROPOSED METHOD PERFORMANCE EVALUATION

A. Actual Data Evaluation

The fault classification method was evaluated with 64 actual oscillographic records with single fault and 2 actual records with crosscountry faults. The records were gathered on CHESF's transmission lines, with different rated voltages (138, 220 and 500 kV) and sampling rates from 1.2 to 15.36 kHz. Five oscillographic data were composed by fault followed by autoreclosure. However, only faults were evaluated in this paper.

Table III summarizes the obtained fault classification results in accordance with the fault types, in which only three oscillographic data with faults were misclassified.

Fig. 8 depicts the fault coordinates obtained in one cycle after fault inception for each actual single fault. The three-phase fault was misclassified because $G(k) > 0.2$, on energy point $k = (k_o + \triangle k)/2$.

TABLE III

PERFORMANCE OF THE FAULT CLASSIFICATION METHOD.

Fault type	Misclassification	Fault type	Misclassification
Falta AG	1/15	Falta AB	0/1
Falta BG	0/26	Falta ABG	0/1
Falta CG	0/18	Falta BC	0/1
Falta AG+ABG	0/1	Falta BCG	1/1
Falta BG+BCG	0/1	Falta ABC	1/1

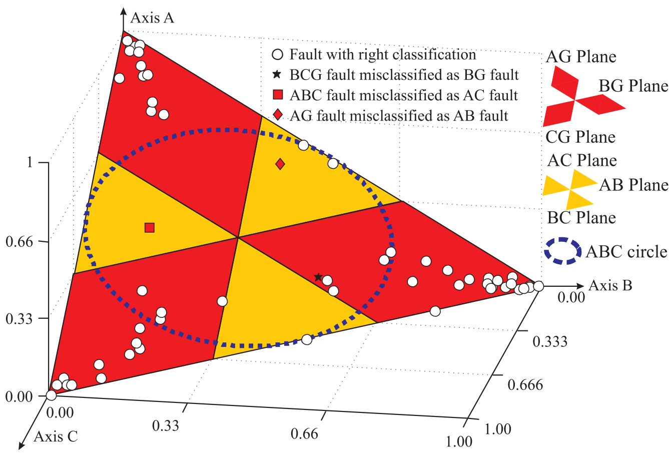

Fig. 8. Fault coordinates for all available actual faults.

Fig. 9 depicts all fault coordinates after fault inception, in two cycles, of the misclassified AG fault. Almost all coordinates of the first cycle after $k_o/2$ were correctly located on AG plane, but the coordinates evaluated by this method were located on AB plane and the fault was misclassified. transient inception on i_B was observed and these transients increased the $\mathcal{E}_B$ magnitude in about one cycle after fault inception. As a consequence, the fault coordinates dropped suddenly to AB plane. As a conclusion, it is possible to evaluate all fault coordinates in one cycle to find the right energy points to reach a success rate of 100 % in all evaluated actual faults.

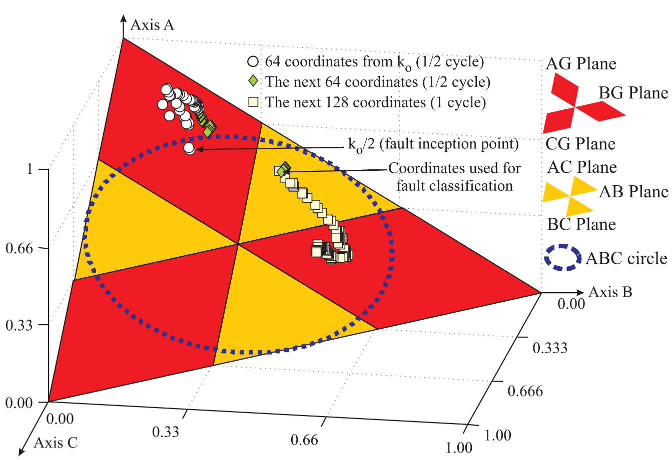

Fig. 9. Fault coordinates in two cycles after fault inception for the misclassified AG fault.

B. Simulated Data Evaluation

Oscillographic data with faults were simulated by using the Alternative Transients Program (ATP) in order to evaluate the fault inception angle, resistance, and location. The system model depicted in Fig. 10 was proposed by [12]. This one is composed by various components: lines, transformers, sources, etc. The transmission lines consist of one pair of mutually coupled lines (between buses 1 and 2), out of which one is a three terminal line. A third line connects Bus 2 to Bus 4. Each 230 kV transmission line is 45 miles long, and there are three sections per line, each section being 15 miles in length. This allows the user to apply faults at various locations. Finally, one monitoring device was inserted in each transmission line terminal (DFR1 to DFR7).

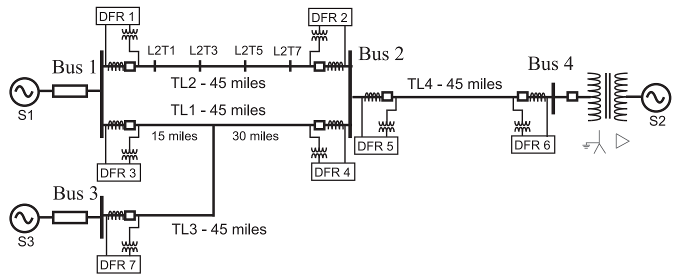

Fig. 10. Power system model proposed by [12].

C. Fault Inception Angle Evaluation

To evaluate the fault inception angle effects, faults on L2T3 section (Fig. 10) were simulated with fault resistance of 50Ω and fault inception angle from 0^o to 180^o, increasing 10^o per time. Oscillographic data with fault by DFR1 (near from fault location) and another one by DFR2 (far from fault location) was obtained for each simulation. In this way, the fault location effects were also evaluated. All fault types were simulated and a total of 380 records were evaluated.

Fig. 11 depicts the fault coordinates in accordance with the fault inception angles for SLG and LL faults. The fault inception angle effects for double phase-to-ground faults are shown in Fig. 12. The SLG and LL faults were rightly classified without distinction for all evaluated fault inception angles and locations (Fig. 11). With regard to DLG faults, some cases were classified as LL faults.

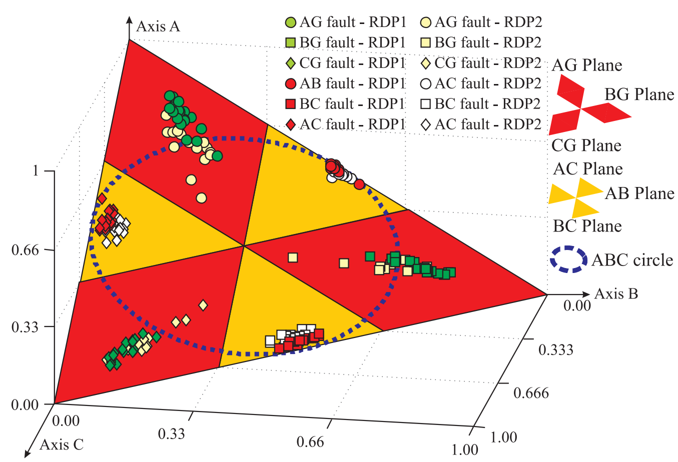

Fig. 11. Fault coordinates for phase-to-phase faults with various fault inception angles.

Fig. 13 depicts the fault inception angle effects on three-phase faults. All faults ware correctly classified ($G(k) < 0.2$). All coordinates are located near the ABC circle (Fig. 13), defined by Eqs. (35), (36) and (37).

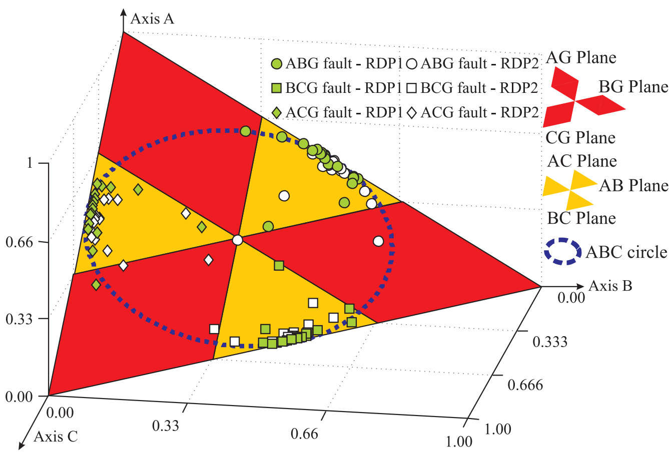

Fig. 12. Fault coordinates for double phase-to-ground faults with various fault inception angles.

D. Fault Impedance Evaluation

In real systems, there is always some damping, which is mostly due to the fault resistance and resistive loads. Damping affects both frequencies and amplitudes of the transients, and then the fault coordinates. The critical fault resistance, at which the circuit becomes overdamped, is in overhead line networks typically 50-200 Ω, depending on the size of the network and also on the fault distance [13].

To evaluate the fault impedance effects, faults on L2T3 section (Fig. 10) with fault inception angle of 30^o and fault resistance of: 1, 10, 20, ..., 90, 100, 150, 200, 250 and 300 Ω were simulated. Oscillographic data with fault by DFR1 (near from fault location) and another one by DFR2 (far from fault location) for each simulation were obtained. In this way, the fault location effects were also evaluated. SLG and LL faults were simulated and a total of 180 records were evaluated. The fault coordinates for these faults are shown in Fig. 14.

According to Fig. 14, the fault coordinates tend to go to the central position of the fault plane with the fault resistance increasing. The obtained results are very promising, because just few recorders with the high resistances in SLG faults were misclassified. On the other hand, the LL faults were correctly classified for all evaluated fault resistances.

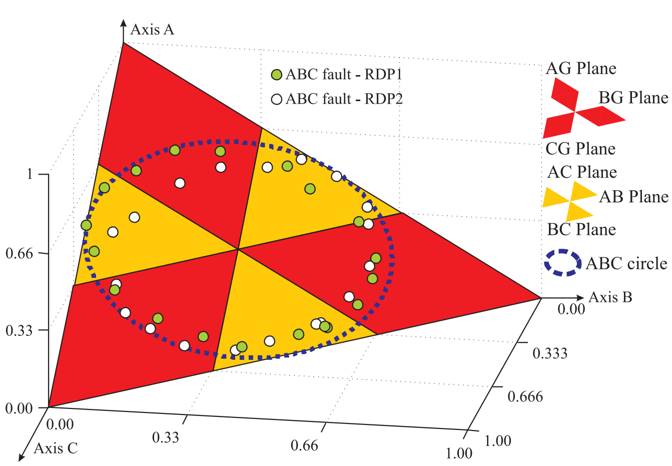

Fig. 13. Fault coordinates for three-phase faults with different fault inception.

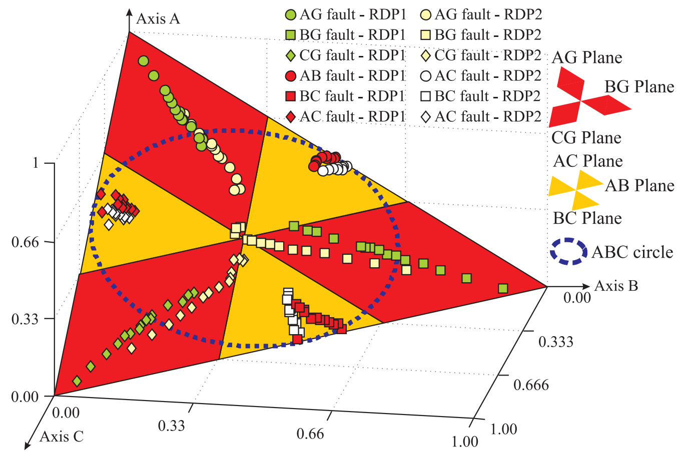

Fig. 14. Fault coordinates for single phase-to-ground faults with various fault resistances.

E. Crosscountry Fault Evaluation

In order to evaluate the fault location, crosscountry faults (AG+ABG faults) on L2T1, L2T3, L2T5 and L2T7 sections (Fig. 10) with fault inception angle of 0, 10, 20, ..., 180 degrees and fault resistance of 10 Ω were simulated. For each simulation, oscillographic data with fault by both DFR1 and DFR2 were obtained. A total of 282 records were evaluated.

Fig. 15 depicts the fault coordinates for the faults located on L2T1 (near the DFR1). The faults gathered by DFR1 were rightly classified in all cases. However, the same AG faults gathered by DFR2 were misclassified due to damping transient effects caused by so far fault location (located on the another transmission line end).

Figs. 16 depicts the fault coordinates for the faults located on L2T3. The faults gathered by both DFR1 and DFR2 were correctly classified in all cases. The same results were obtained by faults located on L2T5.

Fig. 17 depicts the fault coordinates for the faults located on L2T7 (near the DFR2). The faults gathered by DFR2 were correctly classified in all cases. However, few faults gathered by DFR1 were misclassified due to damping transient effects caused by so far fault location.

According to Figs. 15, 16 and 17, the second part of the fault (ABG fault) was correctly classified in all cases.

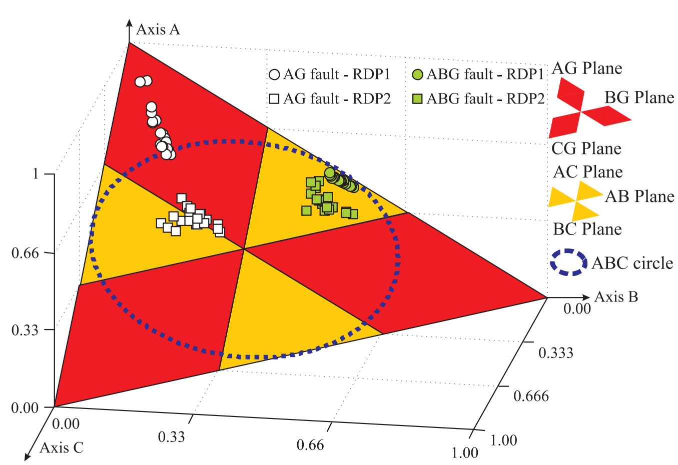

Fig. 15. Coordinates for phase-to-phase faults with various fault resistances.

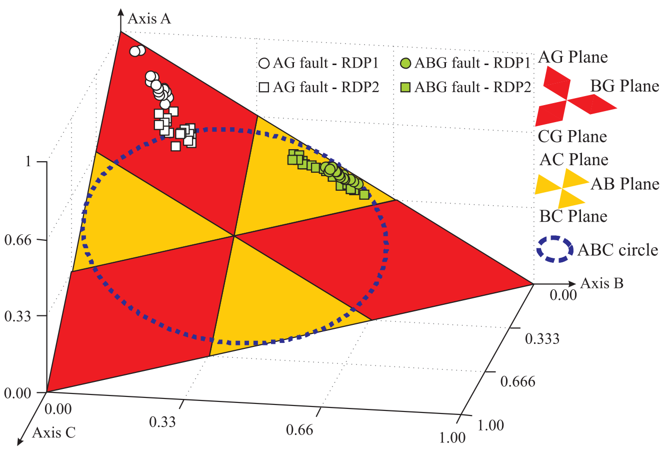

Fig. 16. Coordinates for phase-to-phase faults with various fault resistances.

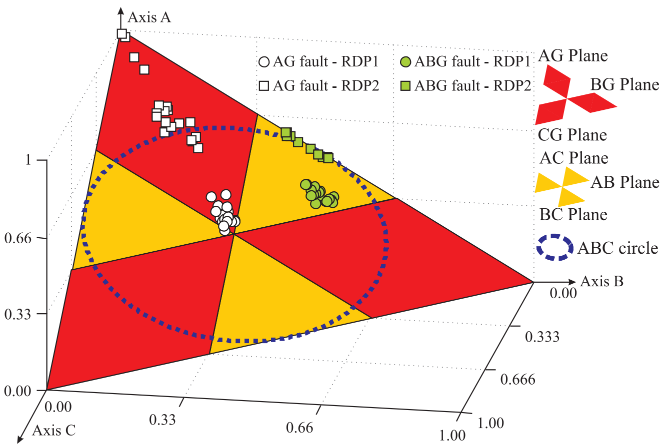

Fig. 17. Coordinates for phase-to-phase faults with various fault resistances.

VI. Conclusions

This paper presents the wavelet coefficient energies as a tool for fault classification in transmission lines. The distinctive feature of the proposed wavelet-based analysis is the ability to classify both single and crosscountry faults.

The proposed method provides the analysis of oscillographic records gathered from different transmission lines with different sampling rates and rated voltages without distinction. The method was based on the wavelet coefficient energies located in one cycle after fault inception. 64 actual records with single faults and 2 actual records with crosscountry faults from various transmission lines of a Brazilian utility were evaluated and good results were achieved. Only three actual single faults were misclassified.

After a post-analysis of the actual faults, it was observed that the firsts energy indexes after fault inception are also suitable for fault classification and it is possible to evaluate all energies in one cycle to reach a better success rate in posterior works.

In order to evaluate the fault inception angle, resistance and location for all kinds of faults, oscillographic data were simulated. A total of 842 simulated records were evaluated and only 19 faults were misclassified.

Almost all misclassified faults in simulated records were related to high impedance fault, obtained by digital fault recorder located on remote transmission line end, with the faults located on the another end.

References

[1] M. Kezunovic and I. Rikalo, “Automating the analysis of faults and power quality,” *IEEE Computer Applications in Power*, vol. 12, no. 1, pp. 46–50, Jan 1999.

[2] C. H. Lee, Y. Juen, and W. Liang, “A literature survey of wavelet in power engineering applications,” *Proc. Natl. Sci. Counc. ROC (A)*, vol. 24, no. 4, pp. 249–258, June 2000.

[3] W. A. Wilkinson and M. D. Cox, “Discrete wavelet analysis of power system transients,” *IEEE Transactions on Power Systems*, vol. 11, pp. 2038–2044, Nov 1996.

[4] O. Poisson, P. Rioual, and M. Meunier, “Detection and measurement of power quality disturbances using wavelet transform,” *International Conference on Harmonics and Quality of Power - ICHQP*, pp. 1125–1130, Athens, Greece, Oct. 1998.

[5] F. B. Costa, K. M. Silva, K. M. C. Dantas, B. A. Souza, and N. S. D. Brito, “A wavelet-based algorithm for disturbances detection using oscillographic data,” *International Conference on Power Systems Transients*, Lyon, France, jun 2007.

[6] O. A. S. Youssef, “Fault classification based on wavelet transforms,” *Transmission and Distribution Conference and Exposition*, vol. 1, pp. 531–536, Nov 2001.

[7] K. M. Silva, B. A. Souza, and N. S. D. Brito, “Fault detection and classification in transmission lines based on wavelet transform and ann,” *IEEE Transactions on Power Delivery*, vol. 21, no. 4, pp. 2058–2063, Oct 2006.

[8] I. Daubechies, *Ten Lectures on Wavelets*. Philadelphia, USA: CBMS-NSF Regional Conference Series, SIAM, 1992.

[9] S. G. Mallat, “A theory for multiresolution signal decomposition: The wavelet representation,” *IEEE Transaction on Pattern Analysis and Machine Intelligence*, vol. 11, no. 7, Jul 1989.

[10] C. H. Kim and R. Aggarwal, “Wavelet transform in power system: Part 2 examples of aplication to actual power system transients,” *Power Engineering Journal*, pp. 193–202, August 2001.

[11] F. B. Costa, B. A. Souza, and N. S. D. Brito, “A wavelet-based algorithm to analyze oscillographic data with single and multiple disturbances,” *IEEE PES General Meeting*, Pittsburgh, USA, jun 2008.

[12] *EMTP Reference Models for Transmission Line Relay Testing*, IEEE POWER SYSTEM RELAYING COMMITTEE, Available on: ¡http://www.pes-psrc.org/Reports-/d6report.zip¿, 2004.

[13] S. Hnninen, “Single phase earth faults in high impedance grounded networks characteristics, indication and location,” Ph.D. dissertation, Helsinki University of Technology, Espoo, Finland, 2001.

F. B. Costa (M’05) was born in Salvador, Brazil, 1978. He received his BS and MS in Electrical Engineering from Federal University of Campina Grande (UFCG), Brazil, in 2005 and 2006, respectively. He is currently a PhD candidate at the same university. His research interest are electromagnetic transients, power quality and fault diagnosis with wavelet transforms and artificial neural network.

B. A. Souza (M’02 - SM’05) received his PhD in Electrical Engineering from Federal University of Paraba, Brazil, in 1995. He works currently as a professor at the Department of Electrical Engineering of Federal University of Campina Grande, Brazil. His main research activities are on optimization methods applied to power systems, electromagnetic transients, power quality and fault diagnostic.

N. S. D. Brito (M’05) was born in Antenor Navarro, Brazil, 1965. She received her BS and PhD in Electrical Engineering from Federal University of Paraba, Brazil, in 1988 and 2001 respectively. She received her MS from Campinas State University, Brazil. She works currently as a professor at the Department of Electrical Engineering of Federal University of Campina Grande, Brazil. Her main research activities are on power quality, especially on applications that involve fault detection and classification in electric systems.